Acta Crystallographica Section F
Structural Biology and Crystallization Communications
ISSN 1744-3091

Crystallization and preliminary X-ray analysis of 6-hydroxymethyl-7,8-dihydropterin pyrophosphokinase from *Staphylococcus aureus*

Sandeep Chhabra,[a,b] Janet Newman,[b] Thomas S. Peat,[b] Ross T. Fernley,[b] Joanne Caine,[b] Jamie S. Simpson[a] and James D. Swarbrick[a]*

[a]Medicinal Chemistry and Drug Action, Monash Institute of Pharmaceutical Sciences, Monash University, 381 Royal Parade, Parkville, Victoria 3052, Australia, and [b]CSIRO Division of Molecular and Health Technologies, 343 Royal Parade, Parkville, Victoria 3052, Australia

Correspondence e-mail: james.swarbrick@pharm.monash.edu.au

Received 19 January 2010
Accepted 23 March 2010

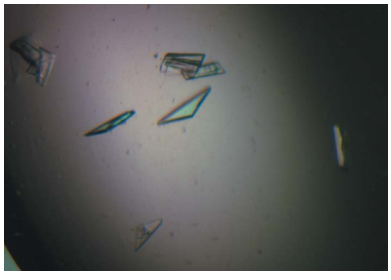

6-Hydroxymethyl-7,8-dihydropterin pyrophosphokinase (HPPK) catalyzes the Mg^{2+}-dependent transfer of pyrophosphate from ATP to 6-hydroxymethyl-7,8-dihydropterin (HMDP), forming 6-hydroxymethyl-7,8-dihydropterin pyrophosphate, which is a critical step in the *de novo* folic acid-biosynthesis pathway. Diffraction-quality crystals of HPPK from the medically relevant species *Staphylococcus aureus* were grown in the presence of ammonium sulfate or sodium malonate and diffracted to better than 1.65 Å resolution. The crystals belonged to space group $P2_1$, with unit-cell parameters a = 36.8, b = 76.6, c = 51.5 Å, $\alpha = \gamma = 90.0$, $\beta = 100.2^\circ$. The crystals contained two molecules per asymmetric unit, with a volume per protein weight (V_M) of 2.04 Å^3 Da^{-1} and an estimated solvent content of 39.6%.

1. Introduction

The increase in rates of bacterial resistance to many antibiotic agents is a major health burden (Cohen, 1992, 1994; Davies, 1994; Neu, 1992; Nikaido, 1994). The number of cases of hospital- and community-acquired *Staphylococcus aureus* infections has grown exponentially together with the parallel emergence of life-threatening 'superbug' methicillin-resistant *S. aureus* (MRSA) strains (Chambers, 2005). Community-aquired strains have become resistant to tetracycline and clindamycin antibiotic treatments (Drew, 2007). In this case, trimethoprim–sulfamethoxazole (TMP–SMX) combination therapy, which synergistically blocks the biosynthesis of folate derivatives by acting on dihydrofolate reductase (DHFR) and dihydrofolate synthase (DHPS), is the main treatment option (Adra & Lawrence, 2004; Proctor, 2008). Resistance to both TMP and SMX has nevertheless emerged, placing a greater burden on vancomycin as an antibiotic of last resort. HIV-infected patients residing in care institutions are a group that is particularly at risk owing to increased exposure to TMP–SMX as an effective *Pneumocystis* treatment (Szumowski *et al.*, 2007). Ever since the introduction of sulfa drugs in the 1930s, their continuing overuse has been blamed for the growing resistance to antibiotics. This is particularly seen to be a problem in developing countries, where overuse is exacerbated by unregulated or inadequate administration. Mechanistically, this has been attributed to several mutations in the DHPS gene. Similarly, with TMP therapy mutations have been observed in the DHFR gene that result in a repositioning of the substrate in the active site (Frey *et al.*, 2009). Thus, with the recent structural data on DHPS and DHFR (Babaoglu *et al.*, 2004; Frey *et al.*, 2009) we are starting to understand the mechanism behind resistance on the atomic level, with the potential to redesign our current chemical approaches. As 6-hydroxymethyl-7,8-dihydropterin pyrophosphokinase (HPPK; EC 2.7.6.3) is not the target of any existing drug, it provides an attractive new folate-pathway target for the rational design and development of novel antimicrobials and antifungals, including those that counter currently resistant isolates.

Folates are essential to all living cells for growth. Accordingly, the enzymes of this pathway (Fig. 1) have been validated as targets for antimicrobials and antifungals. The reduced form of folate, tetrahydrofolate (THF), participates in several important one-carbon transfers that are critical for the biosynthesis of thymidine, glycine

and methionine and vital for DNA replication (Schirch & Strong, 1989). The *de novo* folate-biosynthesis pathway converts 7,8-dihydroneopterin to 7,8-dihydropteroate using ATP and *para*-aminobenzoic acid (*p*ABA). It comprises three committed enzymes, of which HPPK is the second. Initially, dihydroneopterin aldolase (DHNA) catalyzes the epimerization reaction converting 7,8-dihydroneopterin into 6-hydroxymethyl-7,8-dihydropterin (HMDP). HPPK then transfers a pyrophosphate from bound ATP, resulting in 6-hydroxymethyl-7,8-dihydropterin pyrophosphate (HMDPP). DHPS condenses HMDPP with *p*ABA, forming 7,8-dihydropteroate (DHP; Bermingham & Derrick, 2002). The enzymatic addition of glutamate is followed by reduction by DHFR, producing 5,6,7,8-tetrahydrofolate (THF). These latter two reactions are not specific to microbes, plants or protozoa. However, in the case of DHFR structural differences between the human and bacterial enzymes have meant that selective antimicrobials (such as TMP) or, in the case of the human enzyme, cancer treatments such as methotrexate have been successfully deployed.

NMR and X-ray crystal structures of HPPK have been determined from a variety of organisms including *Escherichia coli*, *Haemophilus influenzae*, *Saccharomyces cerevisiae*, *Streptococcus pneumoniae* and *Yersinia pestis* (for reviews, see Swarbrick *et al.*, 2008; Derrick, 2008). Generally speaking, the structures are well conserved and consist of a ferredoxin-like fold comprising a six-stranded β-sheet sandwiched by two α-helices on either side ($\alpha\beta\alpha$ fold). Two Mg^{2+} ions are bound within the active site and these play a major role in the recognition of both the ATP and HMDP substrates. Of the 26 HPPK X-ray and NMR structures that have been deposited, the *S. aureus* homologue shares sequence identities of 39% with the *E. coli*, 39% with the *Y. pestis*, 37% with the *H. influenzae*, 34% with the *S. pneumonia* and 37% with the *S. cerevisae* HPPK enzymes. Much of the understanding of the catalytic mechanism has been deduced from work on the *E. coli* enzyme. In this species, the active-site structure of HPPK is unusually dynamic, as demonstrated by the observation of loop changes in excess of 20 Å throughout the catalytic cycle (Lescop *et al.*, 2009; Blaszczyk *et al.*, 2004). Nevertheless, the high sequence identity of the key active-site residues combined with the high structural similarity of the ternary complexes suggests that inhibitors may have advantageous cross-reactivity potential over different species.

Here, we present a preliminary crystallographic investigation of the *S. aureus* enzyme (*Sa*HPPK) as a prelude towards understanding its catalytic mechanism and as an initial step towards the rational design of novel therapeutics.

2. Materials and methods

2.1. Expression and purification

A pET28a plasmid containing the synthesized *Sa*HPPK sequence (Geneart) was cloned with an N-terminal hexahistidine tag and a thrombin cleavage site. *E. coli* BL21 (DE3) cells transformed with the plasmid were grown overnight in 10 ml 2×YT media supplemented with 100 µg ml^{-1} kanamycin for selection. The overnight culture was then subcultured into fresh 2×YT (1 l) and grown at 310 K until the OD_{600} reached 0.5–0.8. Isopropyl β-D-1-thiogalactopyranoside (IPTG) was added to a final optimized concentration of 0.3 m*M* and expression was carried out at 301 K for 5 h. The cultures were centrifuged at 5000*g* and 278 K for 10 min and the cells were resuspended in 100 ml 50 m*M* HEPES, 5% glycerol pH 8.0. An EDTA-free Complete protease-inhibitor cocktail tablet (Roche) was added together with lysozyme; the latter was added to a final concentration of 0.2 mg ml^{-1}. After 10 min, the cells were sonicated, the cell debris was removed by centrifugation at 18 000*g* for 30 min and the supernatant was filtered (0.45 µm filter).

The supernatant was loaded onto an Ni–NTA IMAC column (Qiagen) and unbound protein was washed off with 10 m*M* imidazole in 50 m*M* HEPES–NaOH buffer, 0.3 *M* NaCl pH 8.0. The tagged protein was eluted from the IMAC column with 250 m*M* imidazole in the HEPES–NaCl buffer; untagged protein was generated by on-column digestion carried out with thrombin to remove the N-terminal His tag. One unit of thrombin (Sigma–Aldrich) was used per milligram of tagged protein. The cleaved protein was eluted from the column with 10 m*M* imidazole in the HEPES–NaCl buffer. Both tagged and untagged versions of the protein were further purified on a Superdex 75 size-exclusion 16/60 column (GE Healthcare) and eluted with 50 m*M* HEPES, 2 m*M* DTT pH 8.0. Fractions were analysed using a 15% SDS–PAGE gel with Coomassie staining and protein-containing fractions were pooled and concentrated to 4.5 mg ml^{-1} using a 3 kDa molecular-weight cutoff ultrafiltration centrifugal device (Amicon). The yields of tagged and cleaved protein were typically ∼35–50 and ∼15–25 mg per litre of culture, respectively. All samples were snap-frozen and stored at 193 K.

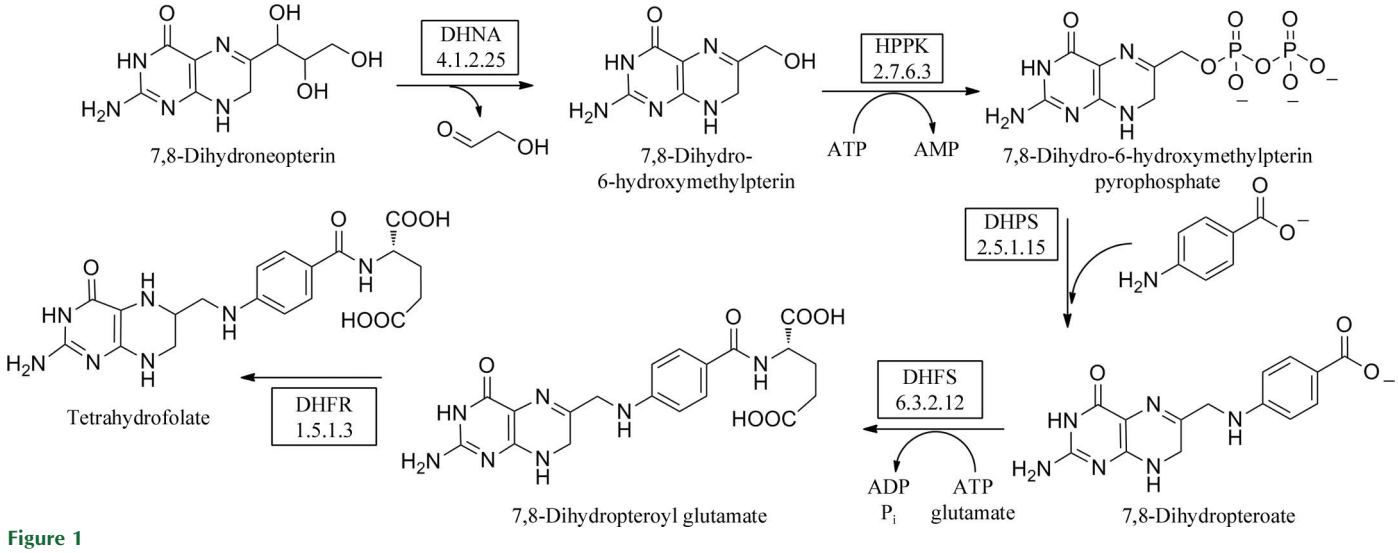

Figure 1
The folate pathway.

2.2. Crystallization

Protein-crystallization experiments (for both the tagged and untagged proteins) were performed at the CSIRO node of the Bio21 Collaborative Crystallization Centre (C3), initially using the PACT and the JCSG+ Suite commercial crystal screens (Qiagen) at 281 and 293 K. A pH *versus* salt gradient screen was also tested at both temperatures. All screens used the sitting-drop vapour-diffusion method with droplets consisting of 250 nl protein solution and 250 nl reservoir solution and a reservoir volume of 50 µl. Crystallizations were performed in SD-2 sitting-drop plates (IDEX Corporation) and were set up using a Phoenix robot (Art Robbins Industries).

Small multiple or twinned crystals were observed after a week in several ammonium sulfate and sodium malonate conditions. A sequential microseeding strategy was employed to improve the size and quality of the crystals. Seeds were created using a seed-bead protocol (Luft & DeTitta, 1999; Newman *et al.*, 2008) and were introduced into the crystallization droplets on setup using the multi-aspirate protocol of a Mosquito robot (TTP Labtech). However, even after several rounds of microseeding optimizations almost all crystals were still partially intergrown. We also tried additive screening with commercially available additive screens (including Additive Screen HT from Hampton Research and The OptiSalt Suite from Qiagen) as well as the addition of different metal ions to find crystallization conditions that would yield single crystals.

2.3. Data collection and analysis

For X-ray data collection, crystals were cryoprotected by adding 1 µl reservoir solution to the droplet and subsequently adding 1.2 µl AP/E Core 150 oil (Mobil-Exxon) to the droplet. Crystals were cryocooled in a nitrogen stream after being pulled through the AP/E oil interface. Data were collected on the microfocus (MX2) beamline of the Australian Synchrotron. 720 images of 0.5° oscillation were collected using an ADSC Quantum 315 detector. The crystal-to-detector distance was 250 mm and the exposure was 1 s for each image. The diffraction data were processed using *MOSFLM* (Leslie, 1992) and *SCALA*/*TRUNCATE* (Collaborative Computational Project, Number 4, 1994). A diffraction pattern of *Sa*HPPK is shown in Fig. 2.

3. Results and discussion

A problem encountered during the crystallization of *Sa*HPPK was a lack of crystal-growth reproducibility owing to batch-to-batch sample variation. This was particularly onerous as the protein would start to precipitate within 24 h of being purified. Therefore, to ensure protein reproducibility in crystallization experiments small aliquots (100 µl) of the freshly purified and concentrated protein were snap-frozen in thin-walled PCR tubes by immersion in liquid nitrogen and then stored at 193 K. The snap-frozen and rapidly thawed protein was used for both screening and optimization experiments, after side-by-side experiments showed that the frozen and thawed sample crystallized as readily and under similar conditions to the fresh protein.

Crystals of the cleaved *Sa*HPPK protein were observed in conditions containing ammonium sulfate (1.4–2.2 *M*) or sodium malonate (1–1.4 *M*) over a wide pH range. Although crystals of the tagged protein were obtained, these crystals did not diffract X-rays well and were not further pursued. Several rounds of serial microseeding were used to improve the crystal quality of the untagged protein. The crystals grown in ammonium sulfate diffracted to 2.4 Å resolution. The ammonium sulfate condition was refined by the addition of different buffers and various metals (Gd, Mn), which improved the

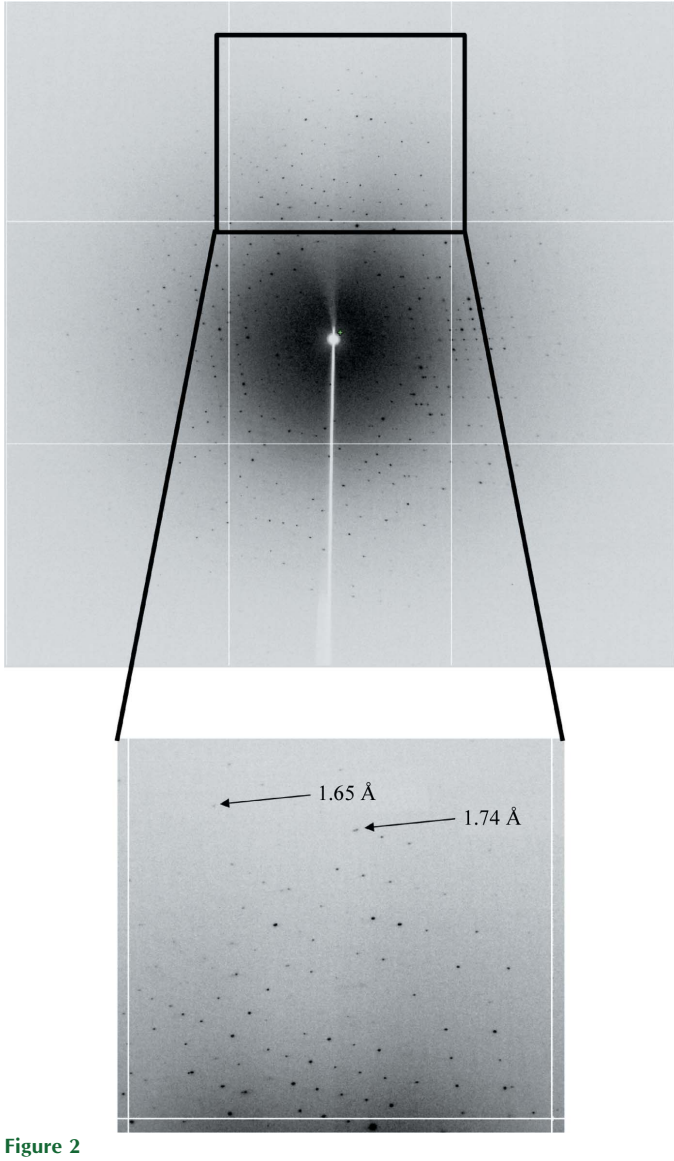

Figure 2
Diffraction image of a typical *Sa*HPPK crystal.

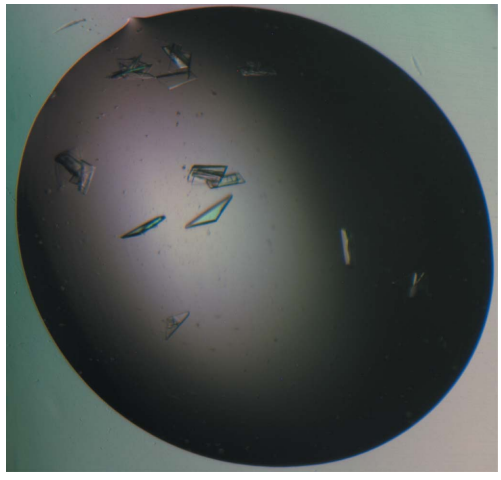

Figure 3
Crystals of *Sa*HPPK. The largest dimension of the central crystal shown is 0.143 mm.

Table 1
X-ray data-collection statistics.

Values in parentheses are for the last shell.

Protein	6-Hydroxymethyl-7,8-dihydropterin pyrophosphokinase (HPPK)
Mass (Da)	18283
Source organism	*S. aureus*
Crystallization method	Sitting-drop vapour diffusion
Temperature (K)	293
Crystal-growth time	Approximately one week
Seeding	Microcrystals
X-ray source	MX2, Australian Synchrotron
Temperature (K)	100
Oscillation angle (°)	0.5
No. of frames used	720
Crystal-to-detector distance (mm)	250
Exposure time (s)	1
Space group	Monoclinic, $P2_1$
Unit-cell parameters (Å, °)	a = 36.8, b = 76.6, c = 51.5, $\alpha = \gamma = 90$, $\beta = 100.2$
No. of molecules in unit cell Z	2
Resolution range (Å)	50.70–1.65 (1.74–1.65)
No. of unique reflections	33864 (4934)
No. of observed reflections	242194
Matthews coefficient V_M (Å^3 Da^{-1})	2.04
Solvent content (%)	39.6
Completeness (%)	100 (100)
Redundancy	7.2 (7.2)
Mean $I/\sigma(I)$	18.3 (4.7)
R_{merge}† (%)	10.22 (0.447)
$R_{p.i.m.}$‡ (%)	4.1 (17.8)

† $R_{merge} = \sum_{hkl}\sum_i |I_i(hkl) - \langle I(hkl)\rangle| / \sum_{hkl}\sum_i I_i(hkl)$. ‡ $R_{p.i.m.} = \sum_{hkl}[1/(N-1)]^{1/2} \times \sum_i |I_i(hkl) - \langle I(hkl)\rangle| / \sum_{hkl}\sum_i I_i(hkl)$, where $I_i(hkl)$ is the observed intensity, $\langle I(hkl)\rangle$ is the average intensity of multiple observations of symmetry-related reflections and N is the redundancy.

diffraction quality of the crystals to about 1.75 Å resolution. We obtained our best diffraction (1.65 Å) from a crystal grown in 1.08 *M* sodium malonate pH 7, 0.09 *M* bis-tris pH 6.5, 0.175 *M* sodium formate, 0.01 *M* sodium acetate pH 4.6 at 293 K. Crystals similar to the one from which data were collected are shown in Fig. 3. Crystals appeared in 5 d and continued to grow to a final maximum length of ∼0.140 mm over a further 15 d. In all, close to 70 96-well plates were set up (over 14 000 droplets); only around ten crystals were tested for diffraction as most of the crystals were too intergrown to be candidates for diffraction studies.

All diffraction data were processed in *MOSFLM*; in all cases the crystals were partially multiple but *MOSFLM* was able to pick out a single diffraction pattern and index these reflections despite the presence of more than one lattice. A data set was collected from a crystal grown in the malonate/formate condition described above and cryoprotected with oil, resulting in a data set which was 100% complete (see Table 1).

The space group was assigned as $P2_1$, with unit-cell parameters a = 36.8, b = 76.6, c = 51.5 Å, $\alpha = \gamma = 90.0$, $\beta = 100.2°$. The overall R_{merge} and $R_{p.i.m.}$ were 10.2% and 4.1%, respectively, V_M was 2.04 Å^3 Da^{-1} and the estimated solvent content was 39.6%. The Matthews coefficient (V_M; Matthews, 1968) suggested the presence of two molecules in the asymmetric unit. Molecular replacement was performed with *Phaser* (Collaborative Computational Project, Number 4, 1994) using the HPPK structure from either *H. influenzae* (PDB code 1cbk; 37% sequence identity; Hennig *et al.*, 1999) or *E. coli* (PDB code 1rao; 39% sequence identity; Blaszczyk *et al.*, 2004) as a search model. Two solutions were found, confirming the presence of two molecules in the asymmetric unit, and model building continues. Both models were tested for their ability to phase the *S. aureus* data as one was in a 'closed' (ATP site unoccupied) form and the other was in a 'open' (ATP-bound) form.

HPPK is a committed enzyme in the folate pathway of *S. aureus* and plays an integral role in the biosynthesis of tetrahydrofolate. The determination of the three-dimensional structure of *Sa*HPPK will be instrumental in the development of novel treatments for community-acquired MRSA infections.

References

Adra, M. & Lawrence, K. R. (2004). *Ann. Pharmacother.* **38**, 338–341.
Babaoglu, K., Qi, J., Lee, R. E. & White, S. W. (2004). *Structure*, **9**, 1705–1717.
Bermingham, A. & Derrick, J. P. (2002). *Bioessays*, **24**, 637–648.
Blaszczyk, J., Shi, G., Li, Y., Yan, H. & Ji, X. (2004). *Structure*, **12**, 467–475.
Chambers, H. F. (2005). *N. Engl. J. Med.* **352**, 1485–1487.
Cohen, M. L. (1992). *Science*, **257**, 1050–1055.
Cohen, M. L. (1994). *Trends Microbiol.* **2**, 422–425.
Collaborative Computational Project, Number 4 (1994). *Acta Cryst.* D**50**, 760–763.
Davies, J. (1994). *Science*, **264**, 375–382.
Derrick, J. P. (2008). *Vitam. Horm.* **79**, 411–433.
Drew, R. H. (2007). *Pharmacotherapy*, **27**, 227–249.
Frey, K. M., Liu, J., Lombardo, M. N., Bolstad, D. B., Wright, D. L. & Anderson, A. C. (2009). *J. Mol. Biol.* **387**, 1298–1308.
Hennig, M., Dale, G. E., D'Arcy, A., Danel, F., Fisher, S., Gray, C. P., Jolidon, S., Muller, F., Page, M. G., Pattison, P. & Oefner, C. (1999). *J. Mol. Biol.* **287**, 211–219.
Lescop, E., Lu, Z., Liu, Q., Xu, H., Li, G., Xia, B., Yan, H. & Jin, C. (2009). *Biochemistry*, **48**, 302–312.
Leslie, A. G. W. (1992). *Jnt CCP4/ESF–EACBM Newsl. Protein Crystallogr.* **26**.
Luft, J. R. & DeTitta, G. T. (1999). *Acta Cryst.* D**55**, 988–993.
Matthews, B. W. (1968). *J. Mol. Biol.* **33**, 491–497.
Neu, H. C. (1992). *Science*, **257**, 1064–1073.
Newman, J., Pham, T. M. & Peat, T. S. (2008). *Acta Cryst.* F**64**, 991–996.
Nikaido, H. (1994). *Science*, **264**, 382–388.
Proctor, R. A. (2008). *Clin. Infect. Dis.* **46**, 584–593.
Schirch, V. & Strong, W. B. (1989). *Arch. Biochem. Biophys.* **269**, 371–380.
Swarbrick, J. D., Iliades, P., Simpson, J. S. & Macreadie, I. (2008). *Open Enzyme Inhib. J.* **1**, 12–33.
Szumowski, J. D., Cohen, D. E., Kanaya, F. & Mayer, K. H. (2007). *Antimicrob. Agents. Chemother.* **51**, 423–428.